Post-AGB Objects and Planetary Nebulae

Michael J. Barlow

Department of Physics & Astronomy,
University College London,
Gower Street, London WC1E 6BT, U.K.

1 Introduction

Planetary nebulae and post-AGB objects are luminous dust emitters in the infrared. Indeed it is by virtue of their strong dust emission that most post-AGB objects (proto-planetary nebulae) have usually been recognised as such, given that the strong optical line emission from photoionized gas that is typical of PNe is absent from the spectra of post-AGB objects, whose central stars occupy the intermediate temperature range between the cool AGB stars and the hot central stars of PNe. Figure 1 shows the characteristic double-peaked optical-IR spectrum of the post-AGB object HD 161796, from Hoogzaad et al. [12]. At optical wavelengths the spectrum of the F3Ib central star dominates, but at IR wavelengths a second peak, due to emission by dust ejected during the earlier AGB phase, is very prominent in its ISO spectrum. Hoogzaad et al. found that contributions from both amorphous and crystalline silicate particles, as well as crystalline water ice were needed to fit the IR spectrum of this oxygen-rich object. Figure 2, from Molster et al. [15], shows the ISO SWS+LWS infrared spectrum of a much more evolved object, the massive bipolar PN NGC 6302. As highlighted in the caption to Fig. 2, a wide variety of C-rich and O-rich particles contribute to its exceedingly rich spectrum.

The focus of this review is however on high spectral resolution IR observations of these objects, so we shall largely neglect the rich literature on broad dust spectral features. In the review I will cover the following topics:

- H_2 spectral surveys of PNe and post-AGB objects; and high spatial and spectral resolution H_2 studies of classic post-AGB objects
- The UIBs in C-rich post-AGB environments and the search for precursors of the UIB carriers
- The possibilities for ultrahigh resolution

2 H_2 studies of planetary nebulae and post-AGB objects

2.1 H_2 spectral surveys of planetary nebulae and post-AGB objects

Two large spectral surveys for H_2 emission from PNe and post-AGB objects have been published in the last few years, by Hora et al. [13] and by Davis et al. [9]. The broad conclusion of these surveys is that H_2 emission is common from post-AGB objects and from old evolved PNe but is rare from intermediate-age luminous
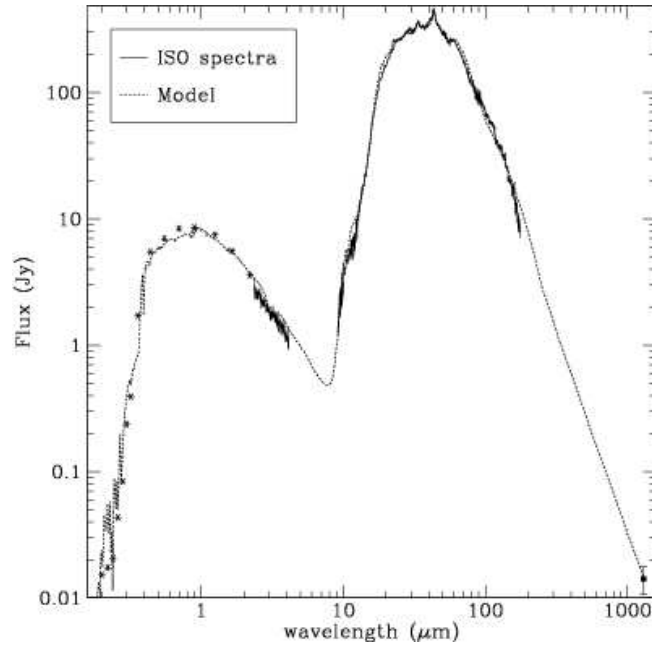
Fig. 1. The optical-IR spectrum of the O-rich post-AGB object HD 161796, from Hoogzaad et al. [12]. This illustrates the classic double-peaked spectrum common to many post-AGB objects.

PNe. As an example, Figure 3 shows the strong H_2 emission spectrum measured by Hora et al. from the archetypal post-AGB objects AFGL 618 and AFGL 2688; the lack of H_2 emission from the bright intermediate age PN NGC 6572; and the very strong H_2 emission from the old PN NGC 6720 (the Ring Nebula).

It seems likely that H_2 emission disappears from intermediate age PNe because any hydrogen remaining in their neutral envelopes has been completely dissociated into its atomic form by the very strong stellar UV radiation field. It has been hypothesised that the H_2 emission seen from many old PNe originates from dense shielded clumps (e.g. the many cometary knots seen in the Helix Nebula) and that these clumps may have survived right through the evolution of the objects. If this is the case, then it is not clear why H_2 emission should not also be seen from intermediate-age objects such as NGC 6572. One possibily is that the dense knots in which H_2 has been detected around old PNe (see Speck et al. [16] for the case of the Helix Nebula) have formed from instabilities in the recombining gas that is left by inward-retreating ionization fronts, as the stellar luminosity declines rapidly as the star joins the white dwarf cooling track.
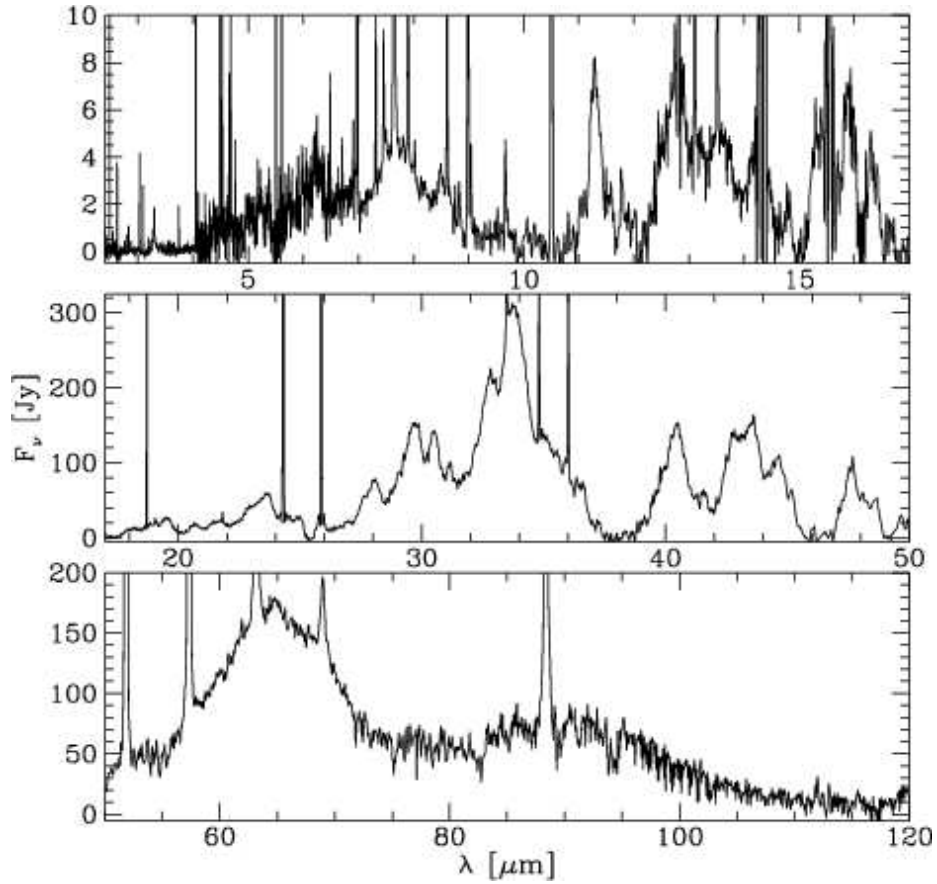
Fig. 2. The ISO 2.4–120-μm spectrum of the bipolar Type I PN NGC 6302, from Molster et al. [15]. The narrow lines are due to various nebular fine structure transitions. The spectrum in the top panel (2.4–17-μm) is dominated by the well-known unidentified infrared bands (UIBs), thought to be due to bending and stretching modes of aromatic hydrocarbon species. The middle panel (17–50-μm) is dominated by relatively sharp emission features that have been associated with crystalline silicates such as fosterite. The 43-μm emission feature of crystalline water ice is also present. The bottom panel (50–120-μm) is dominated by a broad feature, peaking near 65-μm, that has been attributed to a blend of features due to crystalline water ice, diopside and dolomite, while the broad feature at 90-μm has been identified with calcite (Kemper et al. [14]). Both dolomite and calcite are normally thought to require liquid water for their formation.
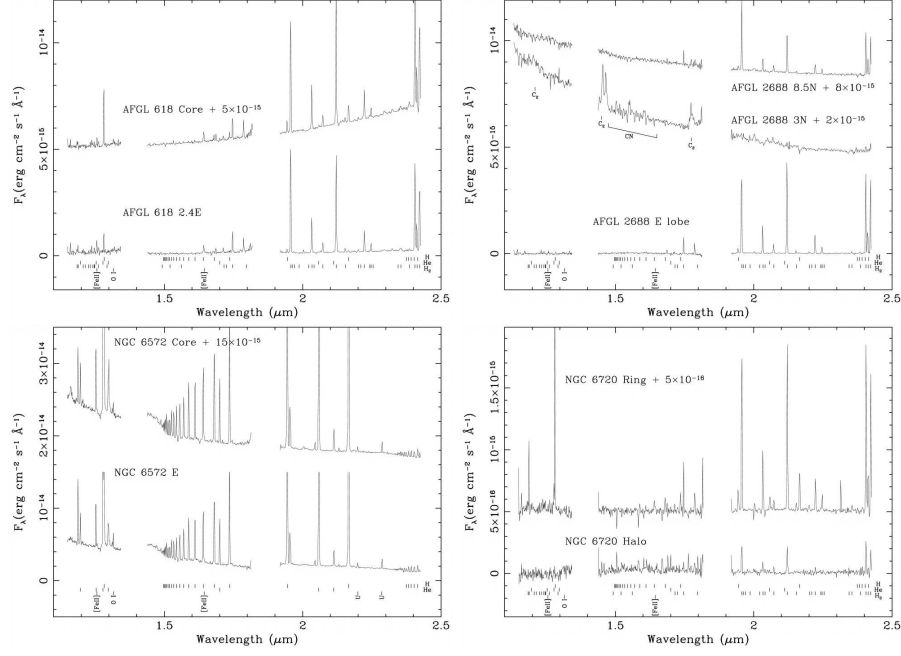
Fig. 3. The JHK spectra of AFGL 618 (top left), AFGL 2688 (top right), NGC 6572 (bottom left) and NGC 6720 (bottom right). Note the strong H_2 emission lines in the 2–2.5-μm spectrum of the two young post-AGB objects (top) and from the old PN NGC 6720, and the lack of such emission from the luminous intermediate-age PN NGC 6572. From Hora et al. [13].

2.2   High spatial and spectral resolution H_2 studies of post-AGB objects

The scientific potential of studies conducted at high spectral **and** high spatial resolution has been demonstrated by a series of papers presenting results obtained at the 3.6-m CFHT with the BEAR near-IR imaging FTS. Cox et al. [7] presented results obtained at 40 km s^{-1} and 0.6 arcsec resolution for NGC 7027 and for the post-AGB object AFGL 2688. Their data allow images to be obtained at any monochromatic wavelength in their spectral coverage, as well as full-band spectra at any position. Figure 4 illustrates some of their results for AFGL 2688. The upper panel shows that the well-known bipolar refelection structure seen at optical and near-IR continuum wavelengths becomes a quadrupolar structure when imaged in the near-IR H_2 lines, while the lower panel shows that the northern and eastern clumps are blue-shifted, while the southern and western clumps are red-shifted, with respect to the systemic velocity. The absence of H_2 emission from the core of GL 2688 seen in the spectra of Hora et al. (Fig. 3), is confirmed by these images. The emission spectrum of the H_2 lines was found by Cox et al. [7] to be consistent with shock excitation.
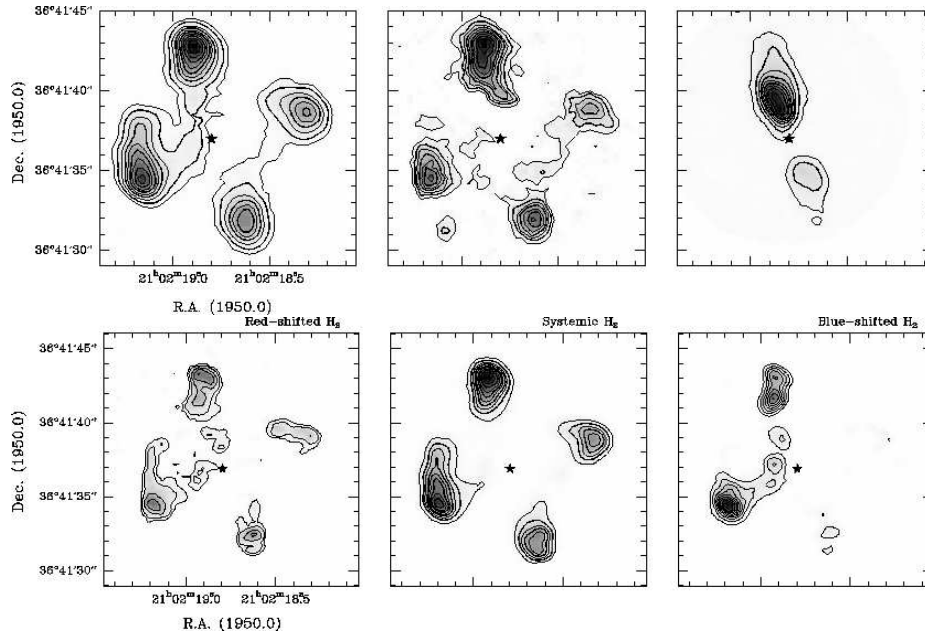
Fig. 4. BEAR imaging FTS maps of AFGL 2688, obtained at the 3.6-m CFHT by Cox et al. [7]. The bipolar reflection nebula seen in optical images and in the K-band continuum (top-right) is replaced by a quadrupolar nebula when imaged in the H_2 1–0 S(1) (top-left) and 1–0 S(0) (top-centre) transitions. The lower panel shows H_2 1–0 S(1) images in selected velocity ranges, demonstrating that the two eastern lobes are predominantly blue-shifted and the two western lobes are predominantly red-shifted, relative to the systemic velocity.

Cox et al. [8] have presented BEAR near-IR results on the post-AGB object AFG 618, obtained at a spatial resolution of 0.5 arcsec and a spectral resolution of 9 km s^{-1}. Figure 5 shows H_2 1–0 S(1) emission images for a number of velocity ranges, superposed upon the HST Hα image of Trammell & Goodrich [17]. The observations reveal the presence of multiple, high-velocity, molecular outflows that are aligned with optical jets seen in the HST image. For previously suggested inclination angles to the line of sight of between 51 and 66 degrees, Cox et al. derived an expnasion velocity of 220–340 km s^{-1} for the H_2 just behind the head of jet b (see middle panel of Fig. 5 for the jet labelling), a factor of 1.8 larger than had previously been estimated from optical line measurements.

3 The search for precursors of the UIB carriers

While the suite of UIBs that are frquently seen in emission in the IR spectra of carbon-rich post-AGB objects and PNe have so far resisted resolution at high spectral resolving powers, searches for light precursor, or fragment, molecules of
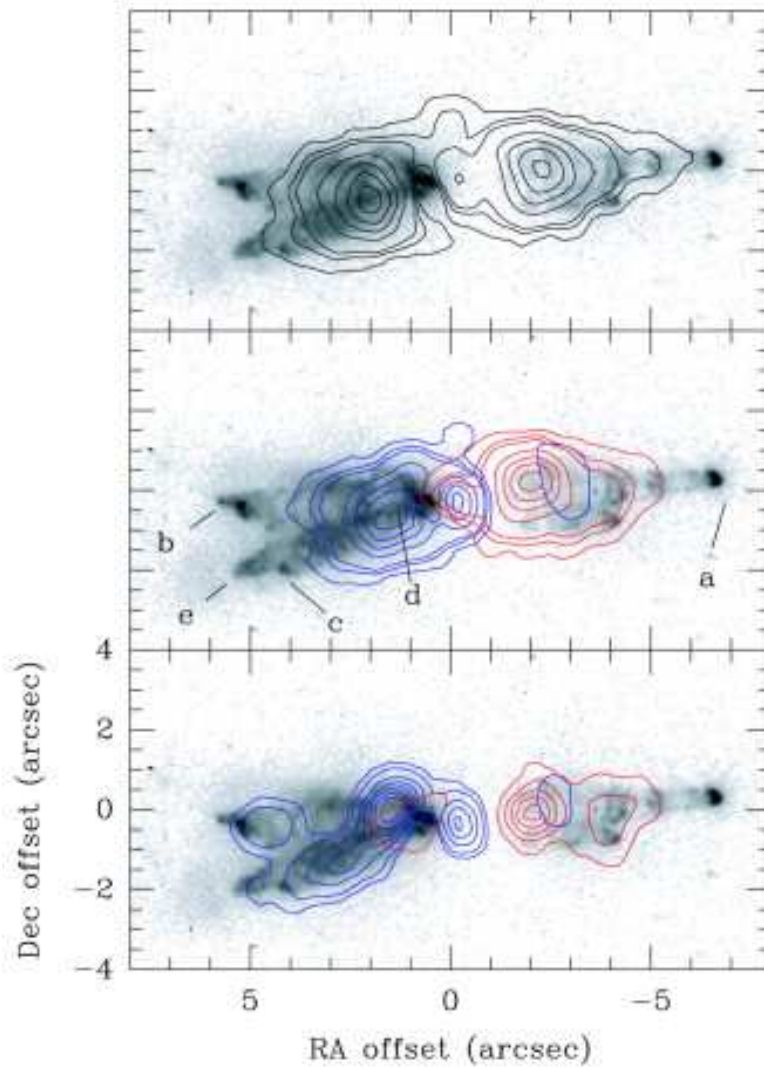
Fig. 5. The contours show H_2 1–0 S(1) emission in selected velocity ranges, superposed upon the HST $H\alpha$ image of Trammell & Goodrich [17]. Top panel: emission around the systemic velocity (–40 to –3 km s^{-1}); middle panel: blue (left) and red (right) intermediate velocities (–41 to –125 and –3 to +81 km s^{-1}); bottom panel: blue (left) and red (right) extreme velocities (–126 to –186 and +82 to +152 km s^{-1}). From Cox et al. [8].

the UIB carriers have been more successful recently. Fig. 6, from Chiar et al. [6] shows how a 3.0–3.1-μm absorption feature in the spectrum of AFGL 618 obtained at a resolving power of 1200 is well matched by a model spectrum for C_2H_2 and HCN in this wavelength region. Clearly, the acquisition of much higher resolution spectra of AFGL 618 in this wavelength region would be justified.
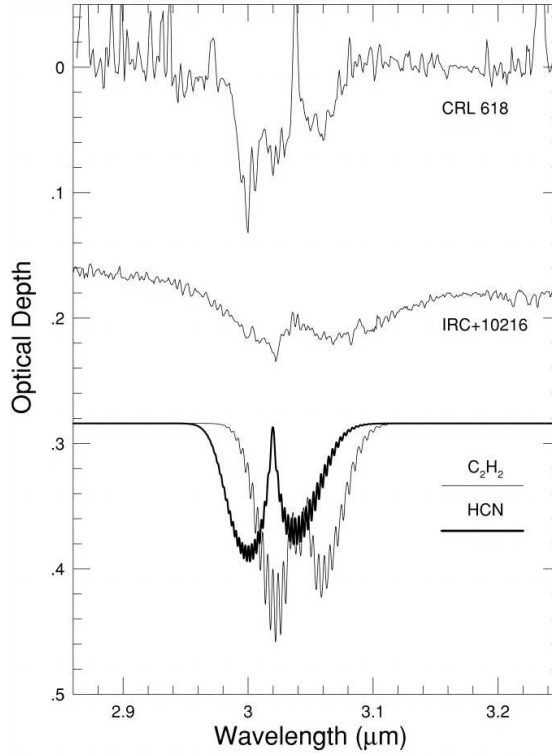

Fig. 6. The UKIRT CGS4 2.9–3.2-μm spectrum of AFGL 618 (upper), obtained at a resolving power of 1200 by Chiar et al. [6]. The middle panel shows the spectrum of the carbon star IRC+10°216 and the lower panel shows a model C_2H_2 + HCN spectrum absorbing at T=200 K, with a line width of 10 km s^{-1}.

Figure 7, from Goto et al. [11], illustrates the similarity between the L-band absorption spectrum of AFGL 618 and the absorption spectrum of the C-rich post-AGB object IRAS 22272+5435 in the same spectral region.

Figure 8, also from Goto et al. [11], shows a comparison between the absorption profile of the 3.3–3.4-μm feature in the spectrum of AFGL 618 and the laboratory absorption spectrum of hydrogen-processed carbon particles, which reproduces the peaks seen at 3.38 and 3.42 μm. These peaks were attributed to asymmetrical vibrational modes of C-H bonds in methyl (3.38 μm) and methylene (3.42 μm) groups.
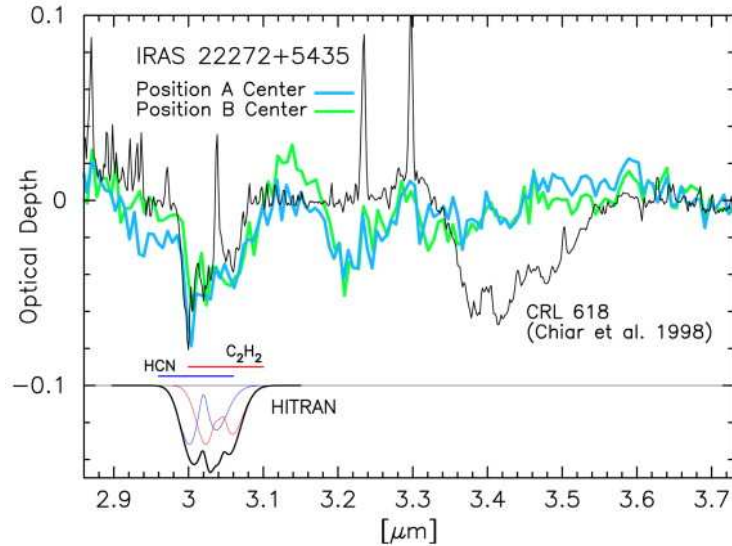
Fig. 7. The 2.9–3.7-μm Subaru IRCS spectrum of IRAS 22272+5435 is compared with that of AFGL 618. From Goto et al. [11].

Cernicharo et al. [4] reported the detection of absorption lines of benzene (C_6H_6) and the polyacetylenic chains C_4H_2 and C_6H_2 in the ISO SWS mid-infrared spectrum of AFGL 618. These bands are visible in Figure 9, taken from [5], which shows the R=1800 7–11-μm ISO SWS spectrum of AFGL 618. Strong absorption bands attributable to ammonia (NH_3) and ethane (C_2H_4) are also present, as are bands due to C_3H_2 and HC_3N. Again, much higher spectral resolution observations are clearly justified for this region of the spectrum of AFGL 618 and other C-rich post-AGB objects.

4   The possibilities for ultrahigh resolution

For pure thermal broadening of a line from a species with atomic weight A and kinetic temperature T, the line FWHM will be $2.14\,A^{-1/2}\,(T/100\,K)^{1/2}$ km s^{-1}. So, for molecular H_2 at temperatures between 100 K and 1000 K, line FWHMs would be between 1.5 and 4.8 km s^{-1} if solely determined by thermal broadening, implying that spectral resolving powers of between 6×10^4 and 2×10^5 are guaranteed to match the H_2 line widths and thereby provide optimum detectivity for weak lines.

From the previous section, we have seen that much heavier species have been detected in absorption in the spectrum of post-AGB objects, e.g. benzene (A=42), ammonia (A=17) and HCN (A=27). If such species produced absorption or emission lines at T=100 K, then the lines would have FWHM widths of 0.50–0.33 km s^{-1} if broadened purely by thermal motions, requiring resolving
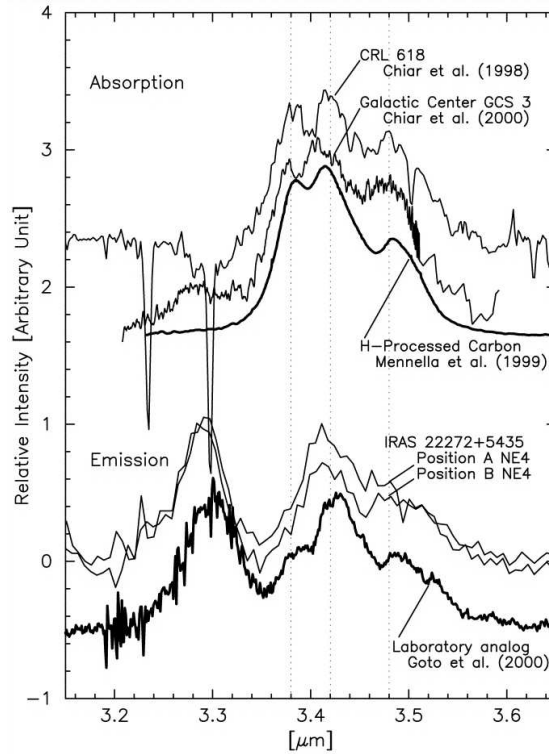
Fig. 8. The upper plots show a comparison between the absorption profiles of the 3.3–3.4-μm features seen towards AFGL 618 and the Galactic Centre source GCS 3, with the laboratory absorption spectrum of hydrogen-processed carbon particles, which reproduces the peaks seen at 3.38 and 3.42 μm. The lower spectra show emission features seen at different spatial positions in the spectrum of IRAS+22272+5435, which are compared to the laboratory spectrum of a thermally annealed hydrocarbon dust. From Goto et al. [11].

powers of 0.5–1.0$\times10^6$ km s^{-1} to match the line widths. Are such narrow line widths plausible? For interstellar lines, the answer is certainly yes, since R=10^6 observations (e.g. Barlow et al. [1], Dunkin & Crawford [3]) have demonstrated that interstellar FWHM line widths can be less than 0.5 km s^{-1}. Shouldn't expansion velocity effects in post-AGB ejecta broaden their circumstellar lines significantly beyond the widths expected from pure thermal broadening? Not necessarily. Observations at a resolution of 0.35 km s^{-1} of circumstellar K I (A=39) 7699 Å absorption components in the spectrum of the C-rich post-AGB star HD 56126 (Crawford & Barlow [2]; see Figure 10) yielded FHWM line widths as low as 0.33 km s^{-1}, implying a rigorous upper limit to the kinetic tempera-ture of the absorbing material of 94 K. Clearly this absorbing material suffers no significant line broadening from velocity gradient effects, implying that the
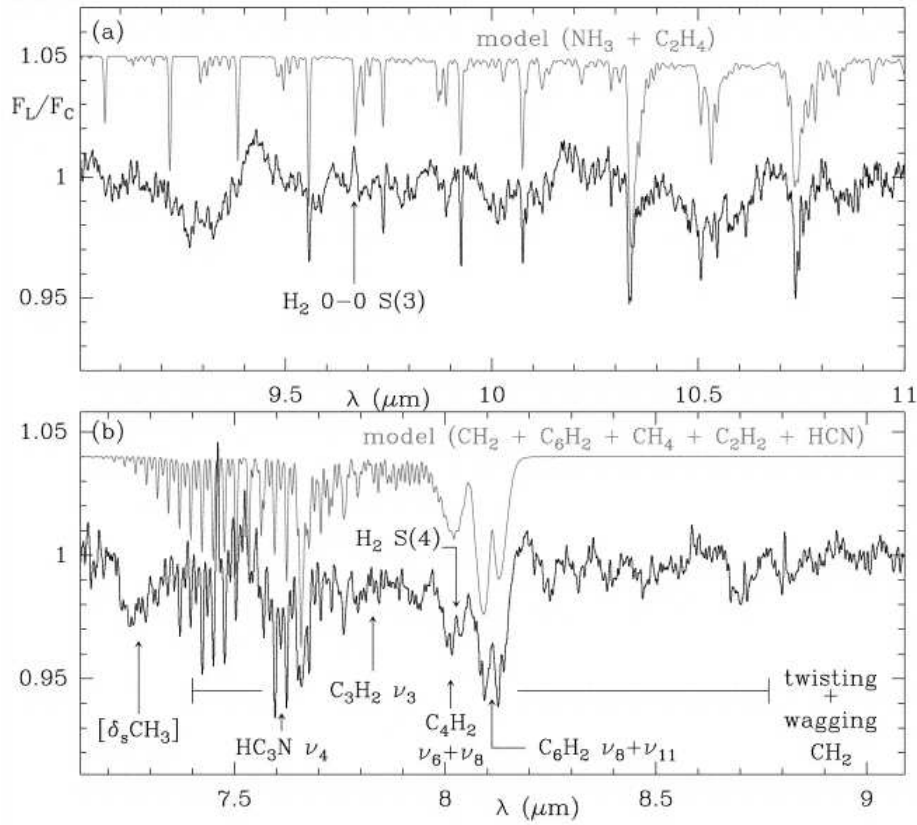
Fig. 9. The ISO SWS grating spectrum of AFGL 618 between 7.0 and 11.0 μm. From Cernicharo et al. [5].
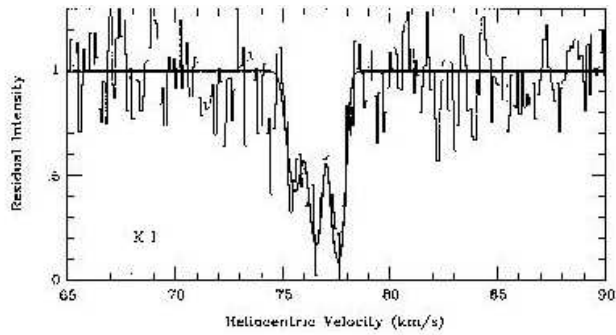

Fig. 10. The circumstellar K I 7699 Å transition observed towards HD 56126. Three circumstellar velocity components are present, with the two narrowest having FWHM line widths of 0.33 km s^{-1}, implying a rigorous upper limit of 94 K to the kinetic temperature of the absorbing gas. From Crawford & Barlow [2].

lines arise from constant velocity ejecta. The relative C_2 rotational level populations, derived by Crawford & Barlow from observations of absorption lines in the 8760 Å region of the spectrum of HD 56126, implied an excitation temperature of only 10 K. Clearly the use of ultrahigh resolving powers of 10^6 or more is justified for future infrared observations of post-AGB objects.

As a final illustration of the potential of ultrahigh resolution in the infrared, Figure 11 shows circumstellar absorption lines from different rotational levels of the ν_3 vibrational band of silane (SiH_4), detected in the 10.5 μm spectrum of IRC+10°216 by Goldhaber & Betz (1984 [10]). They used a heterodyne spectrometer which mixed a tunable CO_2 laser with the input stellar signal onto a HgCdTe photodiode. The difference signal, at radio frequencies, allowed heterodyne detection techniques to be used, automatically yielding very high resolving powers, in this case R=1.5×10^6. Fig. 11 shows the SiH_4 rotational excitation diagram derived by Goldhaber & Betz, from which a rotational temperature of T=173 K was derived.
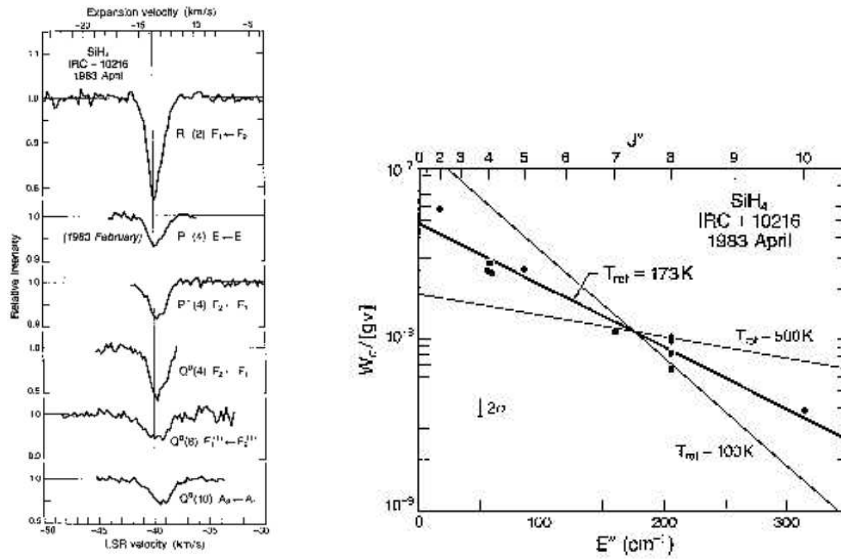

Fig. 11. Left: circumstellar absorption lines from different rotational levels of the ν_3 vibrational band of silane (SiH_4), observed at R=1.5×10^6 in the 10.5 μm spectrum of IRC+10°216 by Goldhaber & Betz [10]. Right: a rotational excitation temperature of 173 K was derived from the relative populations of the absorbing rotational levels of silane.

The narrowest line of SiH_4 (the R(2) transition) observed by Goldhaber & Betz had a FWHM of 1.65 km s^{-1}, implying some degree of velocity gradient broadening relative to the FWHM line width of 0.50 km s^{-1} expected for pure thermal broadening at T=173 K. Since IRC+10°216 is still undergoing stellar

mass loss, such velocity gradient line broadening is to be expected. However, for post-AGB objects the AGB superwind mass loss has ceased, so that constant velocities and narrower, thermally broadened, linewidths should apply, as found for the post-AGB object HD 56126. The infrared heterodyne observations carried out more than 20 years ago by Goldhaber & Betz had limited sensitivity compared to what can be achieved now. With subsequent advances in technology and the availability of significantly larger telescopes, infrared spectroscopy at resolving powers of 10^6 or higher is now feasible for many more targets, including a wide range of post-AGB objects.

References

1. M. J. Barlow, I. A. Crawford, F. Diego, et al.: MNRAS, **272**, 333 (1995)
2. I. A. Crawford, M. J. Barlow: MNRAS, **311**, 370 (2000)
3. S. K. Dunkin, I. A. Crawford: MNRAS, **302**, 197 (1999)
4. J. Cernicharo, A. M. Heras, A. G. G. M. Tielens, et al.: A&A, **546**, L123 (2001)
5. J. Cernicharo, A. M. Heras, J. R. Pardo, et al.: A&A, **546**, L127 (2001)
6. J. E. Chiar, Y. J. Pendleton, T. R. Geballe, A. G. G. M. Tielens: ApJ, **507**, 281 (1998)
7. P. Cox, J.-P. Maillard, P. J. Huggins, et al.: A&A, **321**, 907 (1997)
8. P. Cox, P. J. Huggins, J.-P. Maillard, et al.: ApJ, **586**, L87 (2003)
9. C. J. Davis, M. D. Smith, L. Stern, T. H. Kerr, J. E. Chiar: MNRAS, **344**, 262 (2001)
10. D. M. Goldhaber, A. L. Betz: ApJ, **279**, L55 (1984)
11. M. Goto, W. Gaessler, Y. Hayano, et al.: ApJ, **589**, 419 (2003)
12. S. N. Hoogzaad, F. J. Molster, C. Dominik: A&A, **389**, 547 (2002)
13. J. L. Hora, W. B. Latter, L. K. Deutsch: ApJS, **124**, 195 (2001)
14. F. Kemper, C. Jäger, L. B. F. M. Waters, et al.: Nature, **415**, 295 (2002)
15. F. J. Molster, T. L. Lim, R. J. Sylvester, et al.: A&A, **372**, 165 (2001)
16. A. K. Speck, M. Meixner, D. Fong et al.: AJ, **123**, 346 (2002)
17. S. R. Trammell, R. W. Goodrich: ApJ, **579**, 688 (2002)